frontiers | Frontiers in Control Engineering

TYPE Original Research
PUBLISHED 28 November 2022
DOI 10.3389/fcteg.2022.1055915

Check for updates

OPEN ACCESS

EDITED BY
Yong Xu,
Guangdong University of Technology, China

REVIEWED BY
Danica Rosinová,
Slovak University of Technology in Bratislava, Slovakia
Jun-Wei Wang,
University of Science and Technology Beijing, China

*CORRESPONDENCE
Mohamed Radjeb Oudainia,
Mohamed.Oudainia@uphf.fr

SPECIALTY SECTION
This article was submitted to Networked Control,
a section of the journal
Frontiers in Control Engineering

RECEIVED 28 September 2022
ACCEPTED 14 November 2022
PUBLISHED 28 November 2022

CITATION
Oudainia MR, Sentouh C, Nguyen A-T and Popieul J-C (2022), Online driver model parameter identification using the Lyapunov approach based shared control.
Front. Control. Eng. 3:1055915.
doi: 10.3389/fcteg.2022.1055915

Online driver model parameter identification using the Lyapunov approach based shared control

Mohamed Radjeb Oudainia[1]*, Chouki Sentouh[2], Anh-Tu Nguyen[2] and Jean-Christophe Popieul[2]

[1]LAMIH, CNRS, Univ. Polytechnique Hauts-de-France, Valenciennes, France, [2]LAMIH, CNRS, INSA Hauts-de-France, Univ. Polytechnique Hauts-de-France, Valenciennes, France

The work described in this paper proposes a new conflict minimisation strategy in shared driving control for lane keeping systems (LKS) in intelligent vehicles. This strategy takes into account a dynamic driver model, where the driver's parameters are identified online using the Lyapunov approach. The design of an adaptive shared controller is based on the dynamic parameters of the driver model which changes according to the driver and the situation encountered. Based on Lyapunov stability arguments, the overall asymptotic stability of the closed-loop control system with the adaptive driver model and the variation of the vehicle speed is proved and an LMI optimization is used to formulate the control design. The simulation results, conducted with the SHERPA dynamic car simulator under real-world driving situations, show the importance of integrating a dynamic driver model in the controller design in order to decrease the conflict between the driver and the lane keeping system and to ensure the safety of the vehicle as well as to increase the confidence and acceptability of the driver.

KEYWORDS

driver model parameter identification, advanced driving assistance system, cooperative control, lane keeping control, conflict minimization, adaptive control, identification for control

1 Introduction

Advanced driver assist systems (ADASs) such as lane keeping assist (LKA), adaptive cruise control (ACC), collision avoidance (CA) systems have been widely employed in commercial vehicles. These systems greatly reduce the workload of human drivers and reduce the risk of accidents, and crashes by warning or supporting the driver for particular manoeuvres (Rajamani, 2011). The ADASs developed for semi-autonomous driving scenarios can be categorized into human guided, human supervised and human assisted architectures (Flemisch et al., 2008). In recent works it has been established that driver-in-the-loop (DiL) human assisted ADAS architectures can be employed to address various human machine interaction (HMI) challenges inclusive of authority allocation (Abbink et al., 2011), transition of authority (Saito et al., 2018), conflict management (Nguyen et al., 2017), human driver workload reduction and skill enhancement (Wada et al., 2016). Such cooperative driving architectures have been explored for adaptive cruise control, collision avoidance systems, lane departure/keeping systems among other (Saleh et al., 2013; Schnelle et al., 2017). To design cooperative control architectures for ADAS, DiL architectures are typically formulated by integrating driver attributes such as workload, experience, and skill in the control design. For effective action which reflects such attributes various driver models based on neuromuscular dynamics (Sentouh et al., 2009), data driven (Li et al., 2016), hand impedance (Tanaka et al., 2010), vision/preview model have been developed (Nguyen et al., 2017). In this work, we explore the avenue of cooperative control for Lane Keeping Assist Systems (LKA) by considering the steering input (torque) as a control signal, focusing on the minimization of driver effort as well as the conflict between driver and system. Conflict between the human driver and the autonomous controller typically occurs when both agents have different actions for the same driving task. Such scenarios arise during transition of authority between the agents, sudden manoeuvres executed by driver/automation which is not predicted by the other agent and during extreme manoeuvres i.e. sharp curve negotiation.

1.1 State of the art

Various cooperative control architectures have been proposed in (Saleh et al., 2013; Soualmi et al., 2014; Nguyen et al., 2017; Schnelle et al., 2017; Wang et al., 2017) based on DiL designs. In (Abbink et al., 2011; Mars et al., 2014; Boink et al., 2014) haptic feedback from steering wheel was used to ensure both driver and the autonomous controller participated in the driving action. In (Wada et al., 2016), a co-operative control approach for lane keeping based on H_2 preview control was proposed by incorporating a nuero-muscular driver model. Similarly in (Soualmi et al., 2014), a haptic shared control between driver and e-copilot considered the use of driver torque as haptic feedback to design T-S fuzzy controllers for lane keeping. In (Wang et al., 2017), for varying driver steering characteristics such as delays, and preview time, a DiL gain-scheduling H_∞ robust shared controller was proposed. In, (Wada et al., 2016; Saito et al., 2018) based on cooperative status detection, a conflict free smooth transition of authority between human driver and autonomous controller was proposed. Similarly in (Oudainia et al., 2022), conflict mitigation by adapting the cost function objective was proposed. Extending the work of (Nguyen et al., 2015), a co-operative control approach employing T-S models was proposed in (Nguyen et al., 2017) to perform lane keeping and conflict minimization simultaneously. In (Lv et al., 2018) a haptic control architecture was developed for smooth transition of control authority with adaptation to driver cognitive workload. The works in (Wada et al., 2016; Wang et al., 2017) assumed constant longitudinal speed in the design of lane keeping controllers. Further, conflicts between driver and the automated driving system was not explicitly addressed in (Oufroukh and Mammar, 2014; Wang et al., 2017). In (Nguyen et al., 2018), the unpredictable driver-automation interaction is explicitly taken into account in the shared control scheme, *via* a fictive driver activity variable. Similarly, (Wang et al., 2018) proposed a shared controller for path tracking considering different drivers' characteristics to reduce the physical workloads of the inexperienced drivers. The concept of driver-automation oriented for shared control of lane keeping assist (LKA) was proposed in (Sentouh et al., 2018) based on two local optimal controllers combining system perception with robust control so that the proposed strategy can successfully share the control authority between human drivers and the LKA system. (Pano et al., 2020) presented a shared control strategy with a feedforward-feedback synthesis using a mixed H_2/H_∞ control involving both lane following performance and sharing capabilities indicators. This strategy is interesting as it used the sharing level between the human driver and the assistance explicitly. Moreover, the shared control proposed in (Zhao et al., 2020) is much more flexible since this work follow-up the study in (Pano et al., 2019). It aims to integrate the driver's adaptation in the level of sharing over the driving task using cybernetic driver model. The control authority transition from automated functionality to a human driver is particularly studied in (Lv et al., 2021; Oudainia et al., 2022). This helps drivers to take control of the vehicle progressively. Recently, the shared control strategy have been studied considering driver's behaviors to get a better cooperation. (Huang et al., 2019) presents a cooperative framework developed by adopting data-driven adaptive dynamic programming and an iterative learning scheme based on classical small-gain theory. In (Chen et al., 2020), the lane-keeping control method adopts a driver model based on near and far visual angles with a robust parallel distributed compensation H_∞ controller. These approaches typically validated the cooperative performance of the DiL design for lane keeping tasks. Meanwhile, it is necessary to ensure that this new type of mobility takes into account both driver expectations and foreseeable changes in road user behavior (Sentouh et al., 2009). Overall, the shared control issue being able to share the driving responsibility with human drivers still remains challenging. It is therefore necessary to develop a new Human Machine Interaction strategy (HMI) that allows gradual shared control of vehicle commands between the vehicle and the driver.

1.2 Proposed methodology

Within this work, a novel shared control architecture shown in Figure 1, based on the dynamic of the driver's visual and neruo-muscular parameters which are identified online will be developed and validated in real-time under various driving scenarios with the SHERPA-LAMIH driving simulator. This

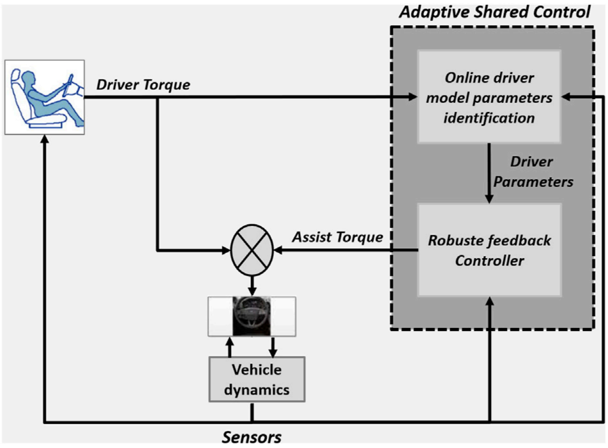

FIGURE 1
Online driver model parameters identification based shared control.

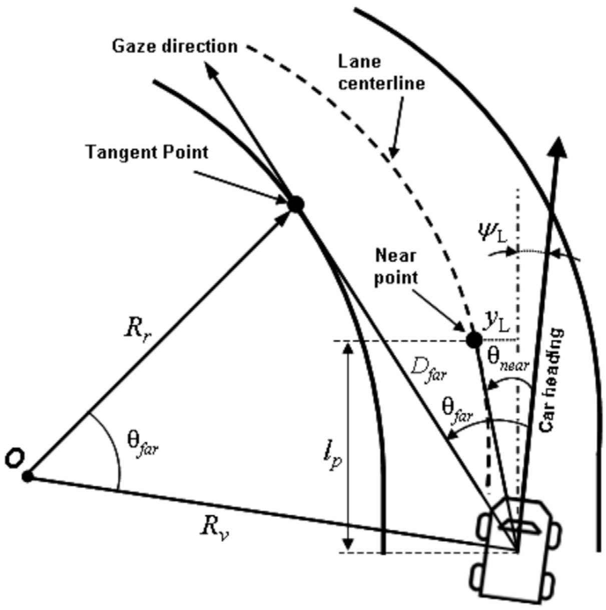

FIGURE 2
Visual angles for anticipatory and compensatory behaviour (Sentouh et al., 2009).

strategy considers the driver's visual and neuro-muscular properties provide an adequate assistance for the driver's abilities. Based on the principle of shared control, the algorithm must ensure the gradual transfer of control from the vehicle to the driver in the safest and most intuitive way for the driver in order to minimize the conflict between them.

The featured contributions of this paper can be summarized in the following aspects:

- A new cybernetic driver model that takes into account the visual and the neuromuscular aspects is proposed (Section 2).
- The parameters of the driver model are estimated online by a new identification approach based on Lyapunov stability (Section 3).
- The aspects of real-time variation in the forward speed and the driver's model parameters properties are treated in a polytope with finite vertices, and treated *via* the boundary domain (Section 4).
- The closed-loop stability of the Driver-Road-Vehicle system with the adaptive driver model and the variation in vehicle speed can be guaranteed using the Lyapunov stability arguments in the LMI control framework (Section 4).

The paper outline is as follows. The Driver-Road-Vehicle modeling is presented in Section 2. The online driver parameters identification approach is shown in Section 3 and the Driver-Automation shared control is designed in Section 4. Subsequently, in Section 5, the performance of the identification approach and the cooperative control scheme is validated in interactive simulation with the well-known SHERPA dynamic car simulator under real-world driving situations.

2 Driver-in-the-loop vehicle modeling

The design of the driver in the loop for cooperative control is carried out in this work for lane keeping, obstacle avoidance, and lane changing maneuvers. For an effective design of the cooperative driver controller, the integrated driver-road-vehicle model is discussed in this section.

2.1 Road-vehicle dynamics

The vehicle lateral dynamics as result of interaction between tires and road surface can be represented by the bicycle model (Rajamani, 2011). The lateral tire friction forces for a vehicle with front steering can be expressed as

$$F_{yf} = 2C_f\alpha_f, \quad F_{yr} = 2C_r\alpha_r$$

where the linear front and rear slip angles are given as follows:

$$\alpha_f = \delta - \beta - \frac{l_f r}{v_x}, \quad \alpha_r = \frac{l_r r}{v_x} - \beta$$

where δ is the wheel angle. The lateral side slip and yaw rate dynamics can be then given as (Sentouh et al., 2018),

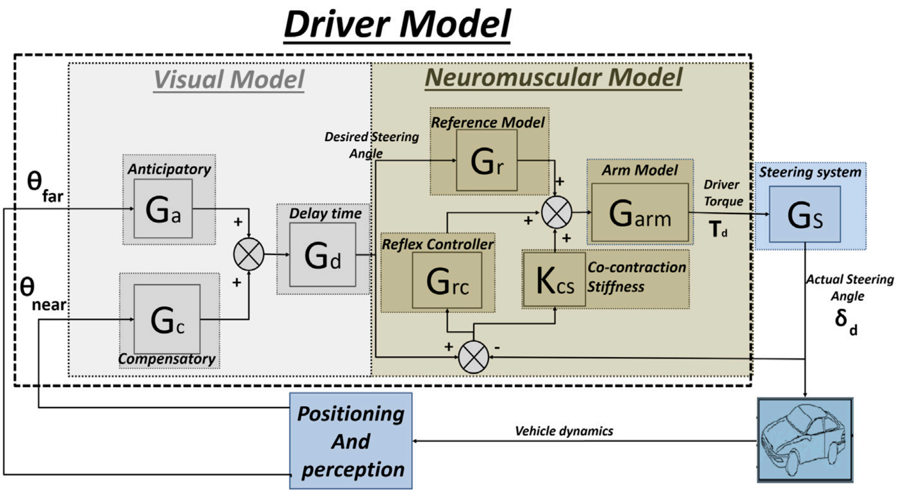

FIGURE 3
Architecture of the proposed driver model.

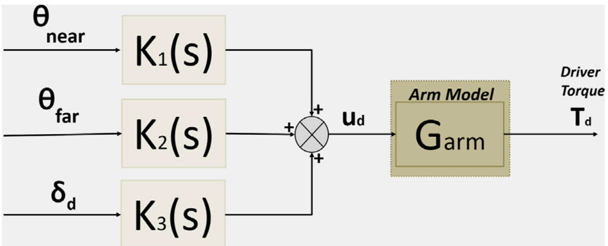

FIGURE 4
Simplified architecture of the proposed driver model.

$$
\begin{cases}
\dot{\beta} = -\dfrac{2\left(C_f + C_r\right)}{mv_x}\beta + \left(\dfrac{2\left(C_r l_r - C_f l_f\right)}{mv_x^2} - 1\right) r + \dfrac{2C_f}{mv_x}\delta + \dfrac{1}{mv_x} f_w \\
\dot{r} = \dfrac{2\left(C_r l_r - C_f l_f\right)}{I_z}\beta + \dfrac{-2\left(C_r l_r^2 + C_f l_f^2\right)}{v_x I_z} r + \dfrac{2C_f l_f}{I_z}\delta + \dfrac{l_w}{I_z} f_w
\end{cases}
\tag{1}
$$

where m is the mass of the vehicle, v_x is the longitudinal velocity, β is the drift angle at the center of gravity, I_z is the vertical moment of inertia of the vehicle, r is the yaw rate, l_f/l_r is the distance between the front/rear axle and the center of gravity of the vehicle, f_w is the lateral wind force having as its center of impact l_w away from the center of gravity. C_f and C_r are the lateral stiffness coefficients of the front and rear pneumatic respectively.

For lane tracking purpose, the vehicle position error y_L and the heading error ψ_L at a look-ahead distance l_p are taken into account in the control design. The dynamics of these variables are given as follows (Sentouh et al., 2018),

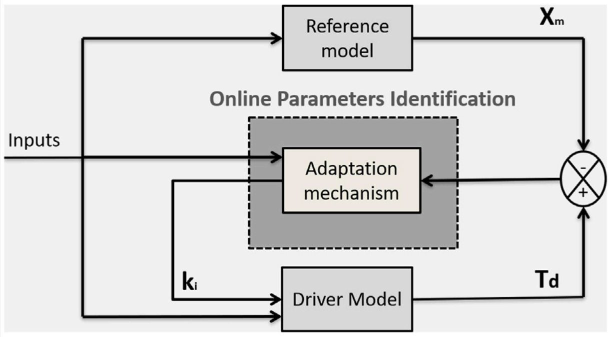

FIGURE 5
Diagram of the online driver parameters identification approach.

$$
\begin{cases}
\dot{\psi}_L = r - \rho_c v_x \\
\dot{y}_L = \beta v_x + l_p r + \psi_L v_x
\end{cases}
\tag{2}
$$

where ρ_c is the curvature of the road. To represent the haptic interaction between the human driver and the vehicle, the dynamics of the steering column is represented as follows,

$$
J_s \ddot{\delta}_d = -B_s \dot{\delta}_d + T_d + T_a - T_s \tag{3}
$$

where δ_d is the steering wheel angle, J_s is the equivalent moment of inertia of the steering system, and B_s is its equivalent damping coefficient. T_d is the driver torque, and T_a is the assisting system torque. Where R_s is the reduction ratio between the steering wheel angle δ_d and the wheel angle δ. The self-aligning torque T_s is expressed as:

FIGURE 6
SHERPA driving simulator.

$$T_s = \frac{-2C_f\eta_t}{R_s}\beta + \frac{-2l_fC_f\eta_t}{R_sv_x}r + \frac{2C_f\eta_t}{R_s^2}\delta$$

where η_t is the width of the tire contact.

2.2 Driver visual-neuromuscular dynamics

It has been shown in the literature that the driver relies on two visual points to guide his vehicle on the road (McRuer et al., 1977; Donges, 1978), a far point allowing him to anticipate the evolution of the curvature and a near point which gives him a compensatory behaviour.

$$\theta_{near} = \frac{y_L}{l_p} + \psi_L, \quad \theta_{far} = D_{far}\frac{r}{v_x} \tag{4}$$

These points can be characterised by the two angles θ_{near} and θ_{far} as used in (Sentouh et al., 2009). The angle θ_{far} represents the angle between the vehicle heading and the tangent to the curve. As for θ_{near}, it represents the angle between the vehicle's heading and the straight line connecting the vehicle's centre of gravity and the point on the edge of the track, located at a distance of l_p as illustrated in Figure 2.In this paper, the driver model proposes to take into account the visual aspect by considering the anticipatory and compensatory behavior of the driver as used in (Sentouh et al., 2009) combined with the neuromuscular aspect as used in (Bi et al., 2015). The architecture of the proposed driver model is shown in Figure 3.

As used in (Sentouh et al., 2009), the visual model consists of three transfer blocks, G_a, G_c and G_d that represent respectively the anticipatory behaviour, the compensatory behaviour and the human processing delay time. In terms of anticipatory control, the driver predicts the future path of the vehicle and provides an anticipated steering input *via* the steering wheel before entering the curve. As for compensatory control, the driver adjusts the torque applied to the steering wheel by using visual information from the region near in front of the vehicle (the near visual angle θ_{near}), in order to keep a safe lateral deviation from the centre of the lane. These transfers are modelled as (Sentouh et al., 2009):

TABLE 1 Values for the vehicle's mathematical parameter model (SHERPA) and for the controller.

Par	Value	Unit
l_f	1.3	m
l_r	1.6	m
l_w	0.4	m
l_p	5	m
η_t	0.13	m
D_{far}	10	m
m	2024	kg
I_z	2,800	$kg.m^2$
J_s	0.05	$kg.m^2$
C_f	57,000	N/rad
C_r	59,000	N/rad
R_s	16	–
B_s	5.73	–
T_n	0.11	s
v_x	[5, 25]	m/s
k_1	[−18, 18]	–
k_2	[−18, 18]	–
k_3	[−18, 18]	–
k_2'	[−0.4, 2]	–
λ	30	–

$$G_a = k_a, \quad G_c = k_c\frac{T_Ls+1}{T_Is+1}, \quad G_d = e^{-\tau_d s} \tag{5}$$

which k_a is the anticipation gain, T_L and T_I are the lead and delay time constants, respectively, and the gain k_c represents the proportional action of the driver with respect to the error of the near visual angle and τ_d is the delay time.

Based on the model used in the (Bi et al., 2015), the neuromuscular model consists of four transfer blocks, G_r, k_{cs}, G_{rc} and G_{arm} which represent respectively the reference model (feed-forward module), the stretch reflex controller, the co-contraction stiffness and the arm model. The reference model represents the angle-torque stiffness, which can provide a steering torque proportional to the desired angle. The co-contraction stiffness refers to the increase in the muscle's intrinsic stiffness resulting from the activation of the muscle. The stretch reflex controller and the arm model represents the dynamics of muscle activation. These transfers are modeled as (Bi et al., 2015) and (Sentouh et al., 2009):

$$G_r = k_r, \quad k_{cs}, \quad G_{rc} = \omega_c\frac{B_rs+K}{s+\omega_c} \quad G_{arm} = \frac{1}{T_ns+1} \tag{6}$$

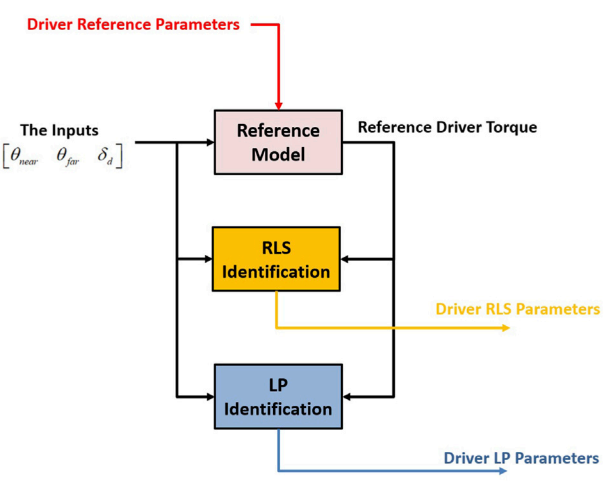

FIGURE 7
Architecture for the comparison of two identification approaches (RLS and LP approach).

which k_r is the feed-forward module, k_{cs} the co-contraction stiffness, K and B_r represent the stiffness and damping of the reflex, respectively, ω_c is the cut-off frequency of the first order filter and T_n is the time constant of the arm system.

In order to design a shared control, the following simplified architecture of the proposed driver model is used:

According to the simplified architecture shown in Figure 4, the following driving model is used:

$$T_d(s) = G_{arm}(s)U_d(s) \tag{7}$$

where $K_1(s)$, $K_2(s)$, $K_3(s)$ and $U_d(s)$ are represented by the following transfer:

$$\begin{cases} K_1(s) = G_c G_d (G_r + G_{rc} + k_{cs}) \\ K_2(s) = G_a G_d (G_r + G_{rc} + k_{cs}) \\ K_3(s) = -(G_{rc} + k_{cs}) \\ U_d(s) = K_1(s)\theta_{near}(s) + K_2(s)\theta_{far}(s) + K_3(s)\delta_d(s) \end{cases} \tag{8}$$

To resume, and from (7) the driver model can be expressed in the form of the following state representation

$$\dot{T}_d(t) = a_d T_d(t) + b_d u_d(t) \tag{9}$$

where $T_d(t)$ is the driver torque, $a_d = -\frac{1}{T_n}$ and $b_d = \frac{1}{T_n}$ are the matrices of the system, and $u_d(t)$ is the driver system input

$$u_d(t) = k_1(t)\theta_{near}(t) + k_2(t)\theta_{far}(t) + k_3(t)\delta_d(t) \tag{10}$$

where the new driver parameters used to design the shared controller are $k_1(t)$, $k_2(t)$ and $k_3(t)$ which represent the compensatory dynamics, the anticipatory dynamics, and the stiffness dynamics of the driver respectively. T_n is a constant, where its value is chosen as in (Sentouh et al., 2009).

In (8), $K_1(s)$, $K_2(s)$, and $K_3(s)$ are transfer functions (in the frequency domain), and in (10) are in the time domain where the latter are unknown (unknown temporal dynamics), so an online parameters identification using a Lyapunov (LP) approach is used to estimate them. This approach will be illustrated in the next section.

2.3 Integrated driver-road-vehicle model

From the dynamics Eqs. 1–3 and Eq. 9 the driver-road-vehicle model can be formulated as follows:

$$\sum: \quad \dot{x} = A(t)x + Bu + Ed \tag{11}$$

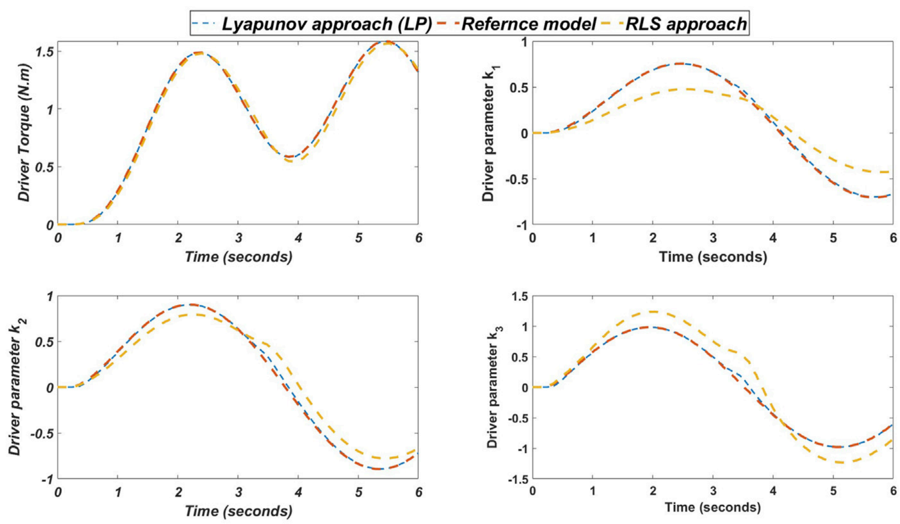

FIGURE 8
The results of the parametric identification by the two approaches (RLS and LP approach).

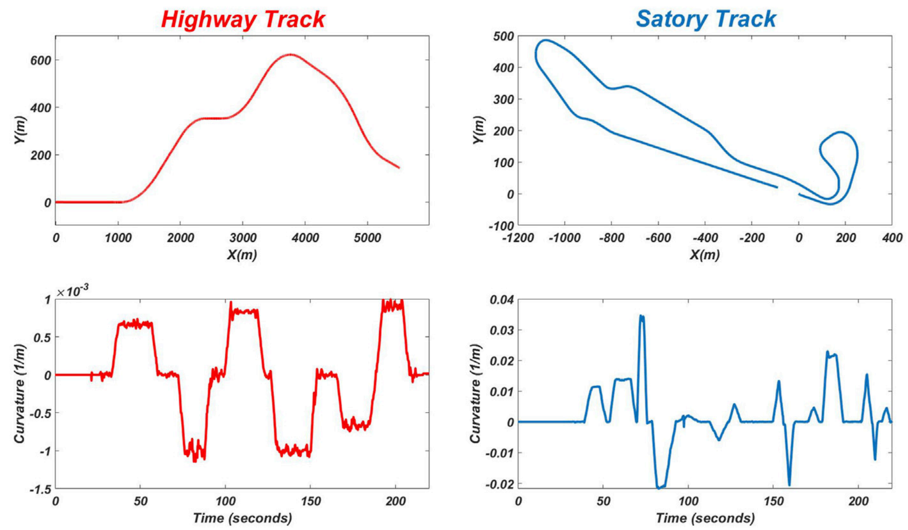

FIGURE 9
The trajectory and curvature for the highway track and the Satory track.

where $x = [\beta \;\; r \;\; \psi_L \;\; y_L \;\; \delta_d \;\; \dot{\delta}_d \;\; T_d]^T$ is the state vector, $u = T_a$ is the control input, $d = [f_w, \rho_c]$ is the disturbance vector, and

$$A(t) = \begin{bmatrix} a_{11} & a_{12} & 0 & 0 & a_{15} & 0 & 0 \\ a_{21} & a_{22} & 0 & 0 & a_{25} & 0 & 0 \\ 0 & 1 & 0 & 0 & 0 & 0 & 0 \\ v_x & l_p & v_x & 0 & 0 & 0 & 0 \\ 0 & 0 & 0 & 0 & 0 & 1 & 0 \\ a_{61} & a_{62} & 0 & 0 & a_{65} & a_{66} & a_{67} \\ 0 & a_{72} & a_{73} & a_{74} & a_{75} & 0 & a_{77} \end{bmatrix},$$

$$B = \begin{bmatrix} 0 & 0 & 0 & 0 & 0 & b_6 & 0 \end{bmatrix}^T,$$

$$E = \begin{bmatrix} e_1 & e_2 & 0 & 0 & 0 & 0 & 0 \\ 0 & 0 & -v_x & 0 & 0 & 0 & 0 \end{bmatrix}^T.$$

with:

$$a_{11} = -\frac{2(C_f + C_r)}{mv_x}, \quad a_{12} = \frac{2(C_r l_r - C_f l_f)}{mv_x^2} - 1, \quad a_{15} = \frac{2C_f}{mv_x R_s},$$

$$a_{21} = \frac{2(C_r l_r - C_f l_f)}{I_z}, \quad a_{22} = -\frac{2(C_r l_r^2 + C_f l_f^2)}{v_x I_z}, \quad a_{25} = \frac{2C_f l_f}{I_z R_s},$$

$$a_{61} = \frac{2C_f \eta_t}{J_s R_s}, \quad a_{62} = \frac{2C_f l_f \eta_t}{v_x J_s R_s}, \quad a_{65} = -\frac{2C_f \eta_t}{J_s R_s^2}, \quad a_{66} = -\frac{B_s}{J_s},$$

$$a_{67} = \frac{1}{J_s}, \quad a_{72} = \frac{k_2'(t) D_{far}}{T_n}, \quad k_2'(t) = \frac{k_2(t)}{v_x}, \quad a_{73} = \frac{k_1(t)}{T_n}, \quad a_{74} = \frac{k_1(t)}{T_n l_p},$$

$$a_{75} = \frac{k_3(t)}{T_n}, \quad a_{77} = -\frac{1}{T_n}, \quad b_6 = \frac{1}{J_s}, \quad e_1 = \frac{1}{mv_x}, \quad e_2 = \frac{l_w}{I_z}$$

3 Online driver parameters identification approach

Our objective is to design an estimator for online parameters identification that guarantees the asymptotic stability of the closed-loop system (Eqs. 9,10) as shown in Figure 5.

The identification scheme consists of three blocks. The first block is the proposed driver model with adjustable parameters Eq. 9. The second block is the adaptation mechanism where it contains the adaptation algorithm used for online parametres identification. The third block represents the reference model, the last one is a black box but it is described by the following equation in order to have the same form as the proposed driving model:

$$\dot{X}_m(t) = a_d X_m(t) + b_d\big(b_1 \theta_{near}(t) + b_2 \theta_{far}(t) + b_3 \delta_d(t)\big) \quad (12)$$

where $X_m(t)$ represents the desired trajectory (the desired driving torque) that $T_d(t)$ in (9) must follow.

In this section we are going to present the adaptation mechanism used for the online parameters identification. We define by $E(t)$ the tracking error $E(t) = T_d(t) - X_m(t)$ which satisfies the following equation

$$\dot{E}(t) = a_d E(t) + b_d\big((k_1(t) - b_1)\theta_{near}(t) + (k_2(t) - b_2)\theta_{far}(t) + (k_3(t) - b_3)\delta_d(t)\big) \quad (13)$$

As adaptation algorithms, we propose:

$$\begin{cases} \dot{k}_1(t) = -\lambda \theta_{near}(t) E(t) \\ \dot{k}_2(t) = -\lambda \theta_{far}(t) E(t) \\ \dot{k}_3(t) = -\lambda \delta_d(t) E(t) \end{cases} \quad (14)$$

with λ it is a positive adaptation parameter.

Theorem 1. Consider the system described by Eq. 9, and a reference model described by Eq. 12 whose input and state variable are bounded. If we apply the system input described by (10) to the system whose parameters are adjusted and identified by the algorithms Eq. 14 then the output of the closed-loop system is bounded for any bounded input signal, and the tracking error converges asymptotically to zero.

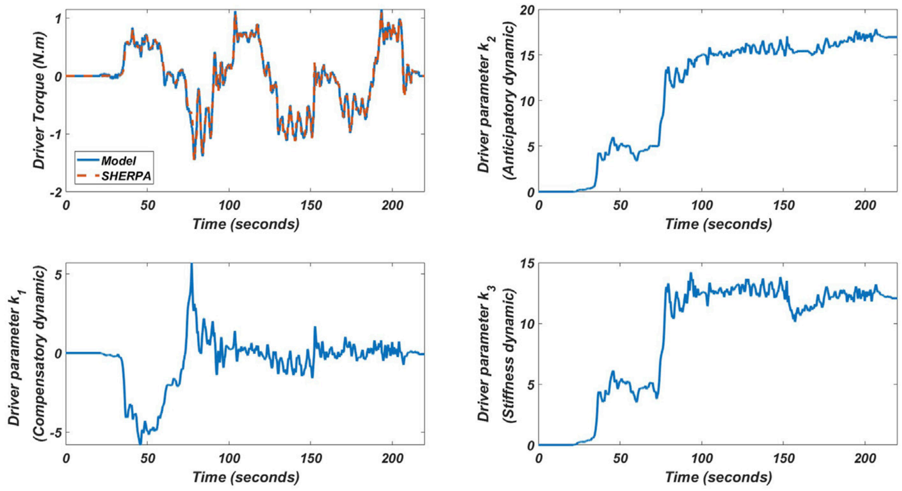

FIGURE 10
The results of the online identification approach of driver parameters in highway track for lane keeping test on the SHERPA simulator.

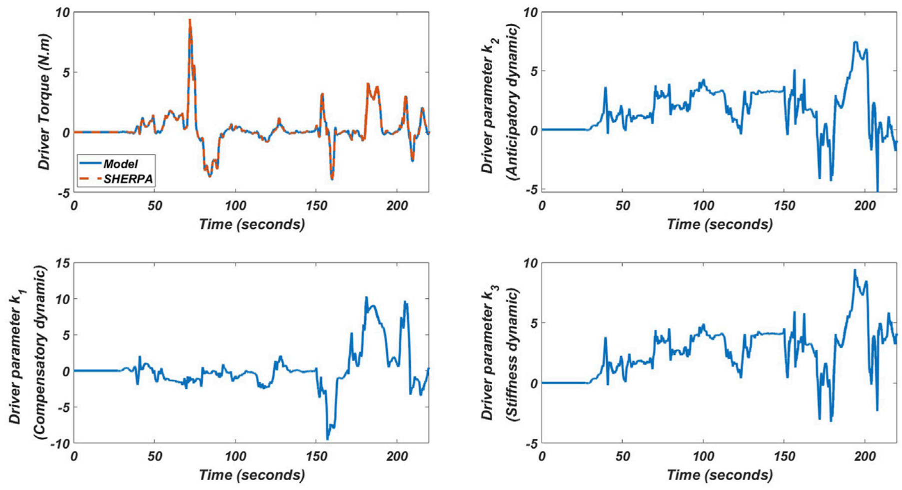

FIGURE 11
The results of the online identification of driver parameters in Satory track for lane keeping test on the SHERPA simulator.

Proof: Let's use the following quadratic Lyapunov function:

$$V = \frac{1}{2}\left(E^2(t) + \frac{b_d}{\lambda}\left((k_1(t) - b_1)^2 + (k_2(t) - b_2)^2 + (k_3(t) - b_3)^2\right)\right) \tag{15}$$

The derivation of the Lyapunov function (15) gives

$$\begin{aligned}\dot{V} = E(t)\dot{E}(t) + \frac{b_d}{\lambda}\Big(&\dot{k}_1(t)(k_1(t) - b_1) \\ &+\dot{k}_2(t)(k_2(t) - b_2) + \dot{k}_3(t)(k_3(t) - b_3)\Big)\end{aligned} \tag{16}$$

replacing (Eq. 13) in (16) and after simplification we obtain

$$\begin{aligned}\dot{V} = a_d E^2(t) + \frac{b_d}{\lambda}\Big(&(k_1(t) - b_1)\big(\dot{k}_1(t) + \lambda\theta_{near}(t)E(t)\big) \\ &+(k_2(t) - b_2)\big(\dot{k}_2(t) + \lambda\theta_{far}(t)E(t)\big) \\ &+(k_3(t) - b_3)\big(\dot{k}_3(t) + \lambda\delta_d(t)E(t)\big)\Big)\end{aligned} \tag{17}$$

By using the adaptation and identification mechanism Eq. 14 we obtain

$$\dot{V} = a_d E^2(t) \tag{18}$$

which is negative semi-definite. This implies that $V(t) \leq V(0)$ and thus that $E(t)$, $k_1(t)$, $k_2(t)$ and $k_3(t)$, are bounded; thus

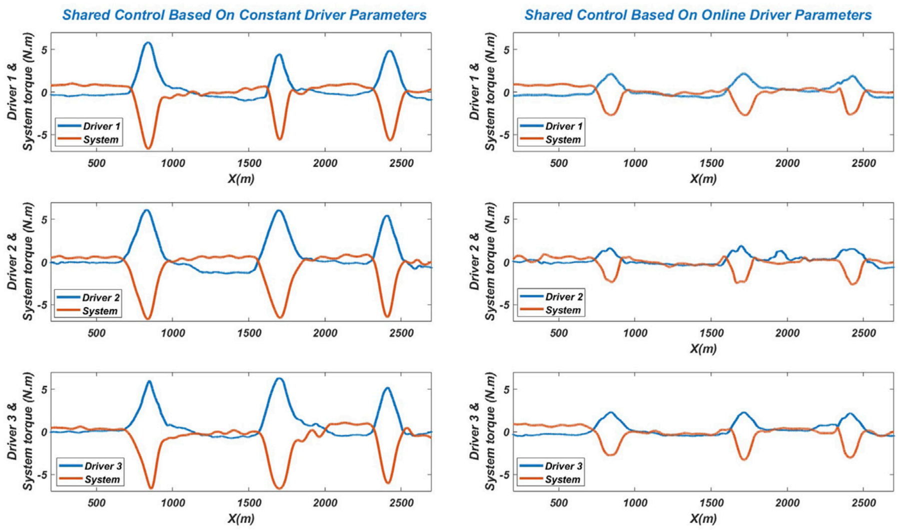

FIGURE 12
The shared controller based on constant and online driver parameters performance of an obstacle avoidance test on the SHERPA simulator.

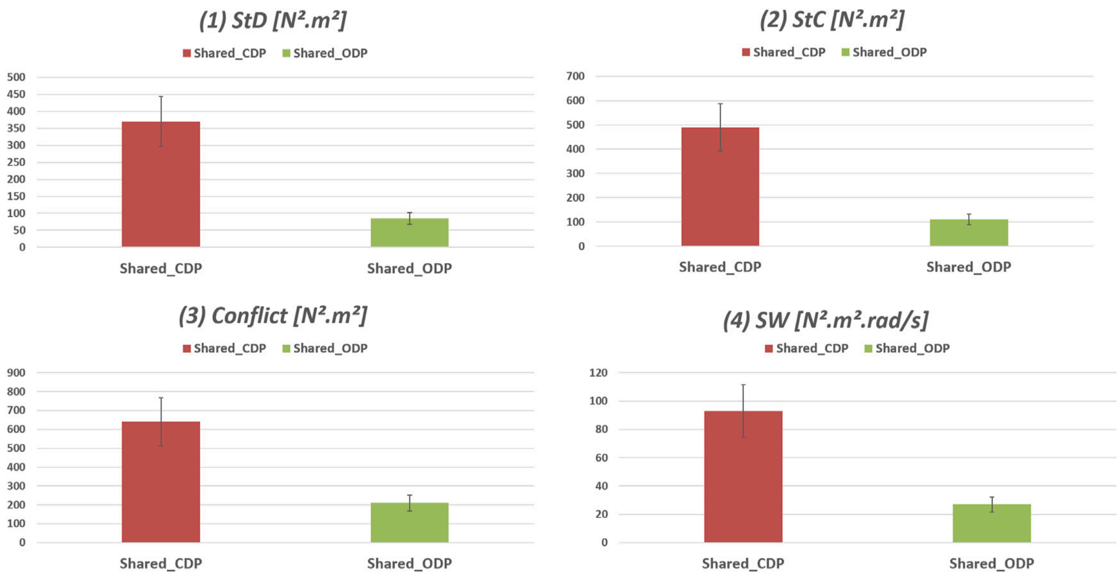

FIGURE 13
Objective evaluation results of the shared controller based on constant and online driver parameters for an obstacle avoidance test on the SHERPA simulator.

$T_d(t) = E(t) + X_m(t)$ is also bounded and when we calculate the second derivative of the Lyapunov function we obtain:

$$\ddot{V} = -2a_d E(t)\dot{E}(t) \tag{19}$$

replacing Eq. 13 in Eq. 19 and after simplification we obtain

$$\ddot{V} = -2a_d E(t)\left(a_d E(t) + b_d\left((k_1(t) - b_1)\theta_{near}(t) + (k_2(t) - b_2)\theta_{far}(t) + (k_3(t) - b_3)\delta_d(t)\right)\right) \tag{20}$$

As the inputs $(\theta_{near}(t), \theta_{far}(t), \delta_d(t))$, $E(t)$ and $T_d(t)$ are bounded then $\ddot{V}$ is bounded, so $\dot{V}$ is uniformly continuous then the error $E(t)$ converges to 0. This concludes the proof.

4 Driver-automation shared control design

This section first presents the T-S fuzzy representation of the integrated driver-in-the-loop vehicle model Eq. 11. Then, we provide in the second subsection an LMI-based solution for the driver-automation shared control problem, and in the last subsection we presents the stability analysis theory of the whole system.

4.1 Fuzzy modeling of driver-in-the-loop vehicle system

Note that A and E in Eq. 11 depend on the following measured, identified and bounded terms:

$$\left\{v_x,\ \frac{1}{v_x},\ \frac{1}{v_x^2},\ k_1,\ k_2',\ k_3\right\}$$

$$\begin{array}{l} v_{\min} \le v_x \le v_{\max} \\ k_{1\,\min} \le k_1 \le k_{1\,\max} \\ k_2{}'_{\min} \le k_2' \le k_2{}'_{\max} \\ k_{3\,\min} \le k_3 \le k_{3\,\max} \end{array}$$

With the approach of sector non-linearity (Wang and Tanaka, 2004), an exact T-S fuzzy model of Eq. 11 can be obtained with $2^6 = 64$ linear sub-systems. However, this vehicle T-S fuzzy model leads to not only expensive numerical burden for real-time implementation but also conservative control results. Here, to reduce significantly the complexity and the conservatism of the proposed control method, the following change of parameter is performed:

$$\frac{1}{v_x} = \frac{1}{v_0} + \frac{1}{v_1}\theta, \quad \theta_{\min} \le \theta \le \theta_{\max} \tag{21}$$

where: $v_0 = \frac{2v_{\min}v_{\max}}{v_{\min}+v_{\max}}$, $v_1 = \frac{2v_{\min}v_{\max}}{v_{\min}-v_{\max}}$. From (21) we obtain:

$$v_x = v_0\left(1 + \frac{v_0}{v_1}\theta\right)^{-1}, \quad \frac{1}{v_x^2} = \frac{1}{v_0^2}\left(1 + \frac{v_0}{v_1}\theta\right)^2$$

Note that the new parameter θ can be used to represent the variation of v_x between its lower and upper bounds, i.e., $\theta_{\min} = -1$, and $\theta_{\max} = 1$. Then, the following first-element Taylor's series around zero is used to exploit the strong relationship between the speed-dependent terms:

$$v_x \approx v_0\left(1 - \frac{v_0}{v_1}\theta\right), \quad \frac{1}{v_x^2} \approx \frac{1}{v_0^2}\left(1 + 2\frac{v_0}{v_1}\theta\right) \tag{22}$$

Remark that v_x, $\frac{1}{v_x}$ and $\frac{1}{v_x^2}$ in Eqs. 21,22 linearly depend on the new parameter θ. Substituting these expressions into Eq. 11, we obtain a vehicle model whose state-space matrices depend on $\{\theta,\ k_1,\ k_2',\ k_3\}$. Using the sector non-linearity approach (Wang and Tanaka, 2004) leads to the following 16-rule T-S fuzzy representation of Eq. 11:

$$\sum:\ \dot{x} = \sum_{i=1}^{2}\sum_{j=1}^{2}\sum_{l=1}^{2}\sum_{m=1}^{2} h_i(\theta)\eta_j(k_1)\mu_l(k_2')\sigma_m(k_3)\left(A_{ijlm}x + Bu\right) + E_i w \tag{23}$$

where A_{ijlm} and E_i are calculated according to:

$$\begin{array}{ll} if\ \ i=1\ \ then\ \ \theta=\theta_{\min}, & if\ \ i=2\ \ then\ \ \theta=\theta_{\max} \\ if\ \ j=1\ \ then\ \ k_1=k_{1\,\min}, & if\ \ j=2\ \ then\ \ k_1=k_{1\,\max} \\ if\ \ l=1\ \ then\ \ k_2'=k_2{}'_{\min}, & if\ \ l=2\ \ then\ \ k_2'=k_2{}'_{\max} \\ if\ \ m=1\ \ then\ \ k_3=k_{3\,\min}, & if\ \ m=2\ \ then\ \ k_3=k_{3\,\max} \end{array}$$

Moreover, the membeT-S fuzzy model are defined as follows:

$$h_1(\theta) = \frac{\theta_{\max} - \theta}{\theta_{\max} - \theta_{\min}}, \quad h_2(\theta) = 1 - h_1(\theta)$$

$$\eta_1(k_1) = \frac{k_{1\,\max} - k_1}{k_{1\,\max} - k_{1\,\min}}, \quad \eta_2(k_1) = 1 - \eta_1(k_1)$$

$$\mu_1(k_2') = \frac{k_2{}'_{\max} - k_2'}{k_2{}'_{\max} - k_2{}'_{\min}}, \quad \mu_2(k_2') = 1 - \mu_1(k_2')$$

$$\sigma_1(k_3) = \frac{k_{3\,\max} - k_3}{k_{3\,\max} - k_{3\,\min}}, \quad \sigma_2(k_3) = 1 - \sigma_1(k_3)$$

4.2 LMI-based design of shared controller

To begin with, we define the performance output of Eq. 11 as

$$z = Cx = \left[\beta\ \ r\ \ \psi_L\ \ y_L\ \ \dot{\delta}_d\ \ T_d\right]^T$$

Note that β, r, ψ_L and y_L represent lane tracking performance while $\dot{\delta}_d$ and T_d are included in z to represent driving comfort and driver effort attenuation respectively. To realize such a shared control scheme, we propose a control solution for the following design problem.

Problem 1. Consider the vehicle model system Eq. 23. Find a controller u such that:

- When $w = 0$, the closed-loop system is globally exponentially stable.
- When $w \neq 0$, the closed-loop system has the input-to-state stability property with respect to the bounded curvature disturbance w.

Furthermore, the following performance index is minimized:

$$\mathfrak{J} = \int_0^\infty \left(z^T(\tau)Qz(\tau) + u^T(\tau)Ru(\tau)\right) \tag{24}$$

For shared control design, we consider the control law:

$$u = \sum_{i=1}^{2}\sum_{j=1}^{2}\sum_{l=1}^{2}\sum_{m=1}^{2} h_i(\theta)\eta_j(k_1)\mu_l(k_2')\sigma_m(k_3)F_{ijlm}x \tag{25}$$

where the control gains F_{ijlm}, $i, j, l, m \in \{1, 2\}$, are to be determined. The following result provides a control solution for Problem 1, where our analysis is conducted using the following Lyapunov function:

$$V(x) = x^T P x, \quad P > 0 \tag{26}$$

Theorem 2. Consider a T-S fuzzy system as described in Eq. 23. The time-varying controller Eq. 25 stabilizes system Eq. 23 while minimizing the performance index Eq. 24 if there exist positive definite matrix X, matrices M_{ijlm}, $i, j, l, m \in \{1, 2\}$, and positive scalars γ, ν, satisfying the following optimization:

Subject to

$$\begin{bmatrix} \nu & x_0^T \\ * & X \end{bmatrix} \prec 0 \tag{27}$$

$$\Gamma_{ijlm} \prec 0, \quad i, j, l, m \in \{1, 2\} \tag{28}$$

where

$$\Gamma_{ijlm} = \begin{bmatrix} He\left(A_{ijlm}x + BM_{ijlm}\right) & E_i & XC^T & M_{ijlm}^T \\ * & -\gamma I & 0 & 0 \\ * & * & -Q^-1 & 0 \\ * & * & * & -R^{-1} \end{bmatrix} \tag{29}$$

Moreover, the feedback gains in Eq. 25 can be computed as follows:

$$F_{ijlm} = M_{ijlm}X^{-1}, \quad i, j, l, m \in \{1, 2\} \tag{30}$$

4.3 Stability analysis

In this subsection, we are going to presents the stability analysis is provided of the whole system.

Proof. Multiplying Eq. 28 with $h_i(\theta) \geq 0$, $\eta_j\ (k_1) \geq 0$, $\mu_l\,(k_2^l) \geq 0$ and $\sigma_m\ (k_3) \geq 0$ and summing up for $\forall i, j, l, m \in \{1, 2\}$ yields

$$\sum_{i=1}^{2}\sum_{j=1}^{2}\sum_{l=1}^{2}\sum_{m=1}^{2} h_i(\theta)\eta_j(k_1)\mu_l(k_2^l)\sigma_m(k_3)\Gamma_{ijlm} \prec 0 \tag{31}$$

For brevity, for any matrices of appropriate dimensions χ_i and Δ_{ijlm}, $\forall i, j, l, m \in \{1, 2\}$ we denote

$$\chi(\theta) = \sum_{i=1}^{2} h_i(\theta)\chi_i,$$
$$\Delta(\theta, k_1, k_2^l, k_3) = \sum_{i=1}^{2}\sum_{j=1}^{2}\sum_{l=1}^{2}\sum_{m=1}^{2} h_i(\theta)\eta_j(k_1)\mu_l(k_2^l)\sigma_m(k_3)\Delta_{ijlm}$$

Using successively Schur complement lemma, it follows that inequality Eq. 31 is equivalent to

$$\begin{bmatrix} \sum_{ijlm} + M(\theta, k_1, k_2^l, k_3)^T RM(\theta, k_1, k_2^l, k_3) + \nabla & E(\theta) \\ * & -\gamma I \end{bmatrix} \prec 0 \tag{32}$$

where $\sum_{ijlm} = He(A(\theta,\ k_1, k_2^l, k_3)X + BM(\theta, k_1, k_2^l, k_3))$, $\nabla = XC^TQCX$. Pre- and post-multiplying Eq. 32 with $P = X^{-1}$, followed by the variable change $M(\theta, k_1, k_2^l, k_3) = F(\theta, k_1, k_2^l, k_3)X$, it follows that

$$\begin{bmatrix} \partial_{ijlm} + F(\theta, k_1, k_2^l, k_3)^T RF(\theta, k_1, k_2^l, k_3) + C^TQC & PE(\theta) \\ * & -\gamma I \end{bmatrix} \prec 0 \tag{33}$$

where $\partial_{ijlm} = He(P(A(\theta, k_1, k_2^l, k_3) + BF(\theta, k_1, k_2^l, k_3)))$. Pre- and post-multiplying Eq. 33 with $[\,x \quad w\,]^T$ and its transpose, it follows that

$$\dot{V}(x) + z^TQz + u^TRu < \gamma w^T w \tag{34}$$

where $\dot{V}(x)$ is the time-derivative of the Lyapunov function candidate Eq. 26 along the trajectory of Eq. 23. From Eq. 34, two following cases are distinguished.

- For free-disturbance system (i.e., w = 0), $\dot{V}(x) < 0$, for $\forall x \neq 0$, this means that system Eq. 23 with controller Eq. 25 is globally exponentially stable.
- For disturbed system (i.e., $w \neq 0$), it follows from Eq. 34 that $\dot{V}(x) < \gamma\|w\|^2$. This guarantees the input-to-state stability property (Sontag and Wang, 1995) of system Eq. 23 with respect to the bounded curvature disturbance w. Moreover, integrating both sides of Eq. 34 over $[\,0 \quad \infty\,]$ yields

$$\mathfrak{I} < V(0) - V(\infty) + \gamma\int_0^{\infty} w(\tau)^T w(\tau)d\tau \tag{35}$$

Since $V(x) > 0$, it follows from (35) that

$$\mathfrak{I} < x_0 P x_0 + \gamma\|w\|_2^2 \tag{36}$$

where $\|w\|_2^2$ denotes the $L2$-norm of w. By Schur complement lemma, it follows from Eq. 27 that $x_0 P x_0 < \nu$ Hence, note from Eq. 36 that Eq. 24 can be minimized by minimizing γ and ν. This concludes the proof.

5 Experimental validation

The experimental validation involves the implementation in a LAMIH road vehicle dynamic simulator SHERPA as illustrated in Figure 6, which is used to demonstrate the effectiveness of the proposed driver model identification approach and the shared control approach. For a better presentation of the paper, this section is divided into two parts, the first part, we are going to validate the driver model and the identification approach by comparing this new approach of identification with the RLS (Recursive Least Square) approach and also validate the model in different test tracks. In the second part, we are going to made a comparison between our shared controller and the shared controller proposed in (Nguyen et al., 2017) for an obstacle avoidance scenario. The values for the vehicle's mathematical parameter model (SHERPA) and for the controller are shown in Table 1, where the limits on k_1, k_2, k_3, and k_2' are obtained experimentally. In order to ensure a faster convergence of the identification system, the value of λ is chosen to be high, in our case ($\lambda = 30$), so that the driver model can quickly converge to the driver action in the case of a rapid change in driver behavior (e.g. from lane keeping to obstacle avoidance).

5.1 Online driver parameters identification performances

This subsection is composed of two parts, the first one consists in the comparison between the proposed identification approach based on Lyapunov (LP) and the RLS approach, and the second part consists in the validation and analysis of the driver behaviour model in different tracks.

5.1.1 Comparison between the proposed identification Lyapunov approach and the RLS approach

In this part, we are going to compare the proposed Lyapunov (LP) identification method with the recursive least square (RLS) method. This comparison is based on a reference model where the model has been created with known varying parameters in order to obtain reference parameters used for the comparison, the identification schema is shown in Figure 7.

The results of the identification by both methods are presented in Figure 8. As we can see, the proposed approach (LP) gives good results compared with that of the RLS method if we look at the tracking of the reference output, i.e. the tracking of the reference driver torque. The explanation of this advantage is shown in the parametric identification results where we can see that the parameters identified by the proposed (LP) approach match with the real reference model parameters compared with the RLS approach. So using (LP) approach will allow us to identify the true parameters of the driver model with the lowest tracking error.

5.1.2 Validation and analysis of the driver behaviour model in different tracks

In order to analyze the behaviour of the driver in different situations, a parametric identification was made in manual driving mode for lane keeping in two different tracks for the same driver. The first track is the highway, with low curvature and a constant speed $v_x = 22\ m/s$, the second track is Satory, with high curvature and a constant speed $v_x = 14\ m/s$. The trajectory and curvature of the two tracks are shown in Figure 9.

The results of the online identification of the driver's parameters for the two tracks (highway and satory) are shown in Figure 10, Figure 11) respectively. As can be seen, the output of the model, i.e. the driving torque, matches perfectly with that of the simulator for both tracks. However, the parametric variation of the driver is not the same for both tests. We can therefore say that the driver's behavior is not fixed but changes according to the situation he meets. It can also be noticed that the driver behaves like a linear model in the first track (highway) i.e. his parameters converge to a constant value compared to the second track where it behaves as a non-linear model. Also we can notice that the parameter which represents the compensatory dynamics in the first track is low compared to the two other parameters, and it can be explained that in the track where the road curvature is low (in a straight line) the driver does not focus much on lane keeping because for him it is easy, so he only gives importance to the other two parameters (anticipation and stiffness). Compared to the second track, where we see that the driver gives importance to the compensation because there are a lot of curves and the road curvature is high.

5.2 Adaptive shared control performance

In this subsection, we are going to made a comparison between our shared controller and the shared controller proposed in (Nguyen et al., 2017), the latter uses a shared control based on a driver model with constant parameters for a lane-keeping scenario (these parameters are obtained offline). This comparison is made in the case of an obstacle avoidance test in highway track, we placed three obstacles and asked three different drivers to avoid them by changing lanes in shared control mode. The test results are shown in Figure 12. It can be seen that the three drivers found it difficult to overtake the obstacle using the controller with constant driver parameters, where the driver and controller torques are high, compared to the proposed shared controller that uses the driver model with estimated parameters online, the three drivers can overtake the obstacle easily without applying high torque. This can be explained by the fact that if we use the same model with constant parameters for obstacle avoidance, the model may be invalid. This result confirms the results obtained in the identification phase shown in Figure 10, Figure 11, where it shows that the driver's behavior changes depending on the situation encountered. All these results show the effectiveness of the proposed method in adapting the shared control to different scenarios and different drivers.

In order to reinforce the results already obtained, an objective evaluation based on metrics to analyse the interaction of the driver with the system and the quality of control was done for the first driver. The interaction is evaluated through the torque exchanged and the angular velocity of the steering wheel during the test phase using the tow controllers, the controller based on constant driver parameters (Shared_CDP) and the proposed controller based on online driver parameters (Shared_ODP). To this end, four indicators were analyzed:

- The total steering effort provided by the driver StED (N.m2 for Steering Effort) during the period of experimentation (T_{Ex}):

$$StED = \int_{T_{Ex}} T_d^2(\tau)d\tau$$

- The total steering effort provided by the controller StEC (N.m2 for Steering Effort) during the period of experimentation (T_{Ex})

$$StEC = \int_{T_{Ex}} T_a^2(\tau)d\tau$$

- The conflict between the driver and the system during the period of experimentation (T_{Ex}):

$$Conflict = \int_{T_{Ex}} |T_a(\tau) - T_d(\tau)|d\tau$$

- SW: This indicates the steering workload and is representative of the effort generated by both agents simultaneously for completing the driving task

$$SW = \int_{T_{EX}} \left|T_a(\tau) \cdot T_d(\tau) \cdot \dot{\delta}_d(\tau)\right|$$

The results of the objective analysis are presented in Figure 13. As we can see, the indicator of the effort provided by the driver and the system using a controller that does not take into account the driver's behavior (Shared_CDP) is high compared to that of (Shared_ODP), this result shows that the proposed controller minimizes the effort applied by the driver in shared control mode and minimize the system effort in order to avoid saturation and overheating of the steering system motor. In addition, even if we compare the conflict indicator, we can clearly see that the (Shared_ODP) minimizes the conflict between the system and the driver in a dynamic way compared to the one that does not take the driver's behavior in consideration (Shared_CDP). Comparing the last indicator, which represents the driving workload, it can be seen that the proposed controller minimizes the workload compared to the (Shared_CDP). So the proposed controller will allow us to minimize the driver effort, the system effort, the conflict between the driver and the system, and the workload on the steering wheel in shared control mode. The obtained results have strongly demonstrated the effectiveness of the proposed shared control method in the attenuation of driver effort and conflict between the lane keeping system and the driver.

6 Conclusion and future works

In this work, a new adaptive cooperative control strategy based on online driver's parameters identification was presented in order to minimize the conflict between the lane keeping system and the human driver. A driver model that takes into account the visual and neuromuscular aspects was presented, where the latter was simplified for the shared control design. Then, a Lyapunov approach was presented for the online identification of driver parameters in order to make the driver model dynamic and personalized to each driver and each situation. The closed-loop stability of the Driver-Road-Vehicle system with the adaptive driver model and the variation in vehicle speed can be guaranteed using the Lyapunov stability arguments in the LMI control framework. The proposed approaches i.e. the identification approach and the shared controller approach are evaluated experimentally using a "full scale" SHERPA car simulator under real-world driving situation in obstacle avoidance scenarios. The obtained results have strongly demonstrated the effectiveness of the proposed shared control method in the attenuation of driver effort and conflict between the lane keeping system and the driver. In future work, we will focus on a polytopic representation with reduced system complexity and with a less conservative fuzzy control law.

Data availability statement

The original contributions presented in the study are included in the article/supplementary material, further inquiries can be directed to the corresponding author.

Author contributions

All the authors listed have made an important contribution, both directly and intellectually, to the work and have approved it for publication.

Funding

This research has been done within the framework of the CoCoVeIA project (ANR-19-CE22-0009-01) funded by the Agence Nationale de la Recherche, the Ministry of Higher Education and Research and the French National Center for Scientific Research.

Acknowledgments

The authors gratefully acknowledge the support of these institutions.

Conflict of interest

The authors declare that the research was conducted in the absence of any commercial or financial relationships that could be construed as a potential conflict of interest.

Publisher's note

All claims expressed in this article are solely those of the authors and do not necessarily represent those of their affiliated organizations, or those of the publisher, the editors and the reviewers. Any product that may be evaluated in this article, or claim that may be made by its manufacturer, is not guaranteed or endorsed by the publisher.

References

Abbink, D. A., Mulder, M., and Boer, E. R. (2011). Haptic shared control: Smoothly shifting control authority? *Cogn. Technol. Work* 14, 19–28. doi:10.1007/s10111-011-0192-5

Bi, L., Wang, M., Wang, C., and Liu, Y. (2015). Development of a driver lateral control model by integrating neuromuscular dynamics into the queuing network-based driver model. *IEEE Trans. Intell. Transp. Syst.* 16, 2479–2486. doi:10.1109/tits.2015.2409115

Boink, R., van Paassen, M. M., Mulder, M., and Abbink, D. A. (2014). "Understanding and reducing conflicts between driver and haptic shared control," in 2014 IEEE International Conference on Systems, Man, and Cybernetics (SMC) (IEEE). doi:10.1109/smc.2014.6974130

Chen, W., Zhao, L., Wang, H., and Huang, Y. (2020). Parallel distributed compensation/h control of lane-keeping system based on the takagi-sugeno fuzzy model. *Chin. J. Mech. Eng.* 33, 61–13. doi:10.1186/s10033-020-00477-9

Donges, E. (1978). A two-level model of driver steering behavior. *Hum. Factors* 20, 691–707. doi:10.1177/001872087802000607

Flemisch, F., Kelsch, J., Loper, C., Schieben, A., Schindler, J., and Heesen, M. (2008). "Cooperative control and active interfaces for vehicle assistance and automation," in FISITA World Automotive Congress.

Huang, M., Gao, W., Wang, Y., and Jiang, Z.-P. (2019). Data-driven shared steering control of semi-autonomous vehicles. *IEEE Trans. Hum. Mach. Syst.* 49, 350–361. doi:10.1109/thms.2019.2900409

Li, L., Liu, Y., Wang, J., Deng, W., and Oh, H. (2016). Human dynamics based driver model for autonomous car. *IET Intell. Transp. Syst.* 10, 545–554. doi:10.1049/iet-its.2015.0173

Lv, C., Wang, H., Cao, D., Zhao, Y., Sullman, M., Auger, D. J., et al. (2018). "A novel control framework of haptic take-over system for automated vehicles," in 2018 IEEE Intelligent Vehicles Symposium (IV) (IEEE). doi:10.1109/ivs.2018.8500480

Lv, C., Li, Y., Xing, Y., Huang, C., Cao, D., Zhao, Y., et al. (2021). Human–machine collaboration for automated driving using an intelligent two-phase haptic interface. *Adv. Intell. Syst.* 3, 2170040. doi:10.1002/aisy.202170040

Mars, F., Deroo, M., and Hoc, J.-M. (2014). Analysis of human-machine cooperation when driving with different degrees of haptic shared control. *IEEE Trans. Haptics* 7, 324–333. doi:10.1109/toh.2013.2295095

McRuer, D. T., Allen, R. W., Weir, D. H., and Klein, R. H. (1977). New results in driver steering control models. *Hum. Factors* 19, 381–397. doi:10.1177/001872087701900406

Nguyen, A.-T., Sentouh, C., Popieul, J.-C., and Soualmi, B. (2015). "Shared lateral control with online adaptation of the automation degree for driver steering assist system: A weighting design approach," in IEEE 54th Annual Conference on Decision and Control (CDC), 857–862.

Nguyen, A.-T., Sentouh, C., and Popieul, J.-C. (2017). Driver-automation cooperative approach for shared steering control under multiple system constraints: Design and experiments. *IEEE Trans. Ind. Electron.* 64, 3819–3830. doi:10.1109/tie.2016.2645146

Nguyen, A.-T., Sentouh, C., and Popieul, J.-C. (2018). Sensor reduction for driver-automation shared steering control via an adaptive authority allocation strategy. *IEEE/ASME Trans. Mechatron.* 23, 5–16. doi:10.1109/tmech.2017.2698216

Oudainia, M. R., Sentouh, C., Nguyen, A.-T., and Popieul, J.-C. (2022). "Dynamic conflict mitigation for cooperative driving control of intelligent vehicles," in 2022 IEEE Intelligent Vehicles Symposium (IV) (IEEE), 1445–1452.

Oufroukh, N. A., and Mammar, S. (2014). "Integrated driver co-pilote approach for vehicle lateral control," in 2014 IEEE Intelligent Vehicles Symposium Proceedings (IEEE). doi:10.1109/ivs.2014.6856519

Pano, B., Zhao, Y., Chevrel, P., Claveau, F., and Mars, F. (2019). Shared control based on an ecological feedforward and a driver model based feedback. *IFAC-PapersOnLine* 52, 385–392. doi:10.1016/j.ifacol.2019.09.062

Pano, B., Claveau, F., Chevrel, P., Sentouh, C., and Mars, F. (2020). "Systematic h 2/h haptic shared control synthesis for cars, parameterized by sharing level," in 2020 IEEE International Conference on Systems, Man, and Cybernetics (SMC) (IEEE).

Rajamani, R. (2011). *Vehicle dynamics and control*. Springer Science & Business Media.

Saito, T., Wada, T., and Sonoda, K. (2018). Control authority transfer method for automated-to-manual driving via a shared authority mode. *IEEE Trans. Intell. Veh.* 3, 198–207. doi:10.1109/tiv.2018.2804167

Saleh, L., Chevrel, P., Claveau, F., Lafay, J.-F., and Mars, F. (2013). Shared steering control between a driver and an automation: Stability in the presence of driver behavior uncertainty. *IEEE Trans. Intell. Transp. Syst.* 14, 974–983. doi:10.1109/tits.2013.2248363

Schnelle, S., Wang, J., Su, H., and Jagacinski, R. (2017). A driver steering model with personalized desired path generation. *IEEE Trans. Syst. Man. Cybern. Syst.* 47, 111–120. doi:10.1109/tsmc.2016.2529582

Sentouh, C., Chevrel, P., Mars, F., and Claveau, F. (2009). "A sensorimotor driver model for steering control," in IEEE International Conference on Systems, Man and Cybernetics (San Antonio, Texas, USA), 2462–2467.

Sentouh, C., Nguyen, A.-T., Benloucif, M. A., and Popieul, J.-C. (2018). Driver-automation cooperation oriented approach for shared control of lane keeping assist systems. *IEEE Trans. Control Syst. Technol.* 27, 1962–1978. doi:10.1109/tcst.2018.2842211

Sontag, E. D., and Wang, Y. (1995). On characterizations of the input-to-state stability property. *Syst. Control Lett.* 24, 351–359. doi:10.1016/0167-6911(94)00050-6

Soualmi, B., Sentouh, C., Popieul, J., and Debernard, S. (2014). Automation-driver cooperative driving in presence of undetected obstacles. *Control Eng. Pract.* 24, 106–119. doi:10.1016/j.conengprac.2013.11.015

Tanaka, Y., Kashiba, Y., Yamada, N., Suetomi, T., Nishikawa, K., Nouzawa, T., et al. (2010). "Active-steering control system based on human hand impedance properties," in 2010 IEEE International Conference on Systems, Man and Cybernetics (IEEE). doi:10.1109/icsmc.2010.5642313

Wada, T., Sonoda, K., and Tada, S. (2016). Simultaneous achievement of supporting human drivers and improving driving skills by shared and cooperative control. *IFAC-PapersOnLine* 49, 90–95. doi:10.1016/j.ifacol.2016.10.467

Wang, H. O., and Tanaka, K. (2004). *Fuzzy control systems design and analysis: A linear matrix inequality approach*. John Wiley & Sons.

Wang, J., Zhang, G., Wang, R., Schnelle, S. C., and Wang, J. (2017). A gain-scheduling driver assistance trajectory-following algorithm considering different driver steering characteristics. *IEEE Trans. Intell. Transp. Syst.* 18, 1097–1108. doi:10.1109/tits.2016.2598792

Wang, J., Dai, M., Yin, G., and Chen, N. (2018). Output-feedback robust control for vehicle path tracking considering different human drivers' characteristics. *Mechatronics* 50, 402–412. doi:10.1016/j.mechatronics.2017.05.001

Zhao, Y., Pano, B., Chevrel, P., Claveau, F., and Mars, F. (2020). "Driver model validation through interaction with varying levels of haptic guidance," in 2020 IEEE International Conference on Systems, Man, and Cybernetics (SMC) (IEEE), 2284.